Non-covalent functionalization of single walled carbon nanotubes with Fe-/co-porphyrin and Co-phthalocyanine for field-effect transistor applications

Fatima Bouanis, Mohamed Bensifia, Ileana Florea, Samia Mahouche-Chergui, Benjamin Carbonnier, Daniel Grande, Céline Léonard, Abderrahim Yassar, Didier Pribat

Non-Covalent functionalization of Single Walled Carbon Nanotubes with Fe-/Co-porphyrin and Co-phthalocyanine for Field-Effect Transistor Applications

Fatima Z. Bouanis[1,2], Mohamed Bensifia[3], Ileana Florea[2], Samia Mahouche-chergui[4], Benjamin Carbonnier[4], Daniel Grande[4], Céline Léonard[3], Abderrahim Yassar[2], Didier Pribat[2]*

[1]COSYS-LISIS, Univ Gustave Eiffel, IFSTTAR, F-77454 Marne-la-Vallée, France
[2]Laboratory of Physics of Interfaces and Thin Films, UMR 7647 CNRS/ Ecole Polytechnique, IPParis, 91128 Palaiseau-France.
[3]MSME, Univ Gustave Eiffel, CNRS UMR 8208, Univ Paris Est Creteil, F-77454 Marne-la-Vallée, France
[4] Univ Paris Est Creteil, CNRS, ICMPE, UMR 7182, 2 rue Henri Dunant, 94320 Thiais

ABSTRACT:

This work reports the non-covalent functionalization of SWNTs with Fe-porphyrin, Co-porphyrin and Co-phthalocyanine molecules. The functionalized SWNTs were first characterized using Raman and X-ray photoelectron spectroscopies. Observations down to nanoscale resolution were also performed by atomic force microscopy, as well as scanning and transmission electron microscopies. The spectroscopic methods evidenced an electronic interaction between the metal-centered molecules and the SWNTs, ensuring the robustness of the functionalization. High resolution microscopy characterizations reveal that the porphyrin and phthalocyanine molecules are adsorbed on the surface of SWNTs. The electrical characterizations show a weak charge transfer between those grafted molecules and the

Corresponding Authors

Fatima Zahra Bouanis**:** *Univ Gustave Eiffel, IFSTTAR, F-77454 Marne-la-Vallée, France*
Tel: +33 (0) 1 69 33 43 85, E-mail address: fatima.bouanis@ifsttar.fr

SWNTs, confirming the electronic interaction between the molecules and the SWNTs. Density functional theory (DFT) supports experimental data and helps understanding the experimental results of selective interaction of metal complexes with one type of semiconducting SWNTs.

Keywords: SWNTs, CNTFETs, Noncovalent functionalization, Porphyrin, Phthalocyanine

1. Introduction

Single-walled carbon nanotubes (SWNTs) have attracted much attention due to their outstanding physical, chemical and mechanical properties [1-2]. These properties, make them a potential material for the development of new applications, especially when SWNTs are incorporated in new functional materials [3]. Considerable efforts have been devoted to the chemical functionalization of SWNTs [4]. In this context, the combination of SWNTs with new functional group offers new functionalities, which are particularly appealing for applications in the areas of solar energy conversion [5], electronic and sensing devices [6] as well as for new biological applications [7]. The functionalization of SWNTs with appropriate compounds led to the development of new nano-hybrid materials. These new systems not only provide various original chemical functionalities and optoelectronic properties, but also have the potential to be employed in functional devices for energy and electronic applications. As an example, SWNTs functionalized with metallophthalocyanines (MPc) and metalloporphyrin (MPo), have shown a high chemical stability, as well as unique physicochemical, physical and structural properties [8-10]. In addition to their unique structural and original properties, they are quite easy to prepare [11]. There is a rich literature on the modification of SWNTs with MPo and MPc [11-15]. The first example of nano-hybrid materials of SWNTs and MPo was published by Nakashima and co-workers [16]. In their work, they reported that the Van der Walls interactions act as a driving force for nano-hybrid formation [16]. Both covalent and non-covalent approaches have been employed to

functionalize SWNTs with MPo [11-15]. The non-covalent functionalization allows reliable immobilization of molecules on the surface of SWNTs, while preserving their intrinsic properties [6, 13, 17]. Covalent modification, however offers strong and stable anchoring of functional groups but it has the limitation of destroying the extended π-system of SWNTs, which provokes the loss of some of their properties [14, 18-19].

Previous work has reported physisorption properties of iron porphyrin on both metallic and semiconducting CNTs. The kinetic and thermodynamic properties of non-covalently bound CNT/porphyrin oligomers have been investigated by UV/visible spectroscopy and fluorescence titration. It was found that the affinity of these molecules to adsorb on the CNTs surface increases sharply with the porphyrin coverage, showing strongest binding energies for semiconductor-type CNTs [20]

To fully explore the new functionalities of SWNTs, a modified carbon nanotube field-effect transistor (CNTFET) device configuration is the best suited device to probe the charge transport properties. Although CNTFET based on a network of SWCNTs functionalized with MPc and MPo for sensing applications have been studied for decades, several challenges still remain, such as a lack of advanced morphological characterizations at nanoscale, including the interface between the grafted molecules and the SWNTs, the homogeneity of the adsorption of the molecules on the nanotube surface, and the chemical mapping with nanoscale resolution. Understanding how the experimental conditions affect the molecular adsorption or how they influence the molecule/SWNT properties, in order to improve the selectivity or CNTFET gas sensors, are also remaining challenges to explore.

We study herein the non-covalent assembly of MPo and MPc onto CNTFETs via physi-adsorption and π-π interactions, and its characterization in order to obtain accurate chemical, structural, and morphological information, by the combined use of high-resolution transmission electron microscopy (HRTEM), X-Ray photoelectron spectroscopy (XPS) and

electrical measurements. This family of molecules possesses a planar structure with a large π system, facilitating π-π interaction with the SWNTs surface, without destroying the electronic properties of CNTFETs, which makes them good candidates for non-covalent functionalization. Two types of MPo, namely 5,10,15,20-Tetraphenyl-21H,23H-porphryine cobalt(II) (Co-Por) and 5,10,15,20-Tetraphenyl-21H,23H-porphyrine iron (III) chloride (Fe-Por) as well as cobalt (II) phthalocyanine (Co-Phc) were used for the surface functionalization of SWNTs. The SWNTs were synthesized on SiO_2/Si substrates from Ru catalyst nanoparticles, using double hot filament chemical vapor deposition (d-HFCVD) [21]. The composition and the structure of the resulting nanohybrid materials are characterized by spectroscopic methods such as Raman spectroscopy and XPS, and also by microscopy-type methods such as scanning microscopy (SEM)-energy-dispersive spectroscopy (EDS), transmission electron microscopy (TEM) and atomic force microscopy (AFM). The results indicate that these molecules strongly bind to the side walls of SWNTs. The electrical measurements showed a slight change in the I-V characteristic of Fe-Por/CNTFETs, Co-Por/CNTFETs and Co-Phc/CNTFETs devices. This slight change can be attributed to a charge transfer between the metal-centered molecules and SWNTs, which confirms the non-covalent bonding of these molecules to the SWNTs. This is supported by a theoretical study that evidences that the molecules are electron donors and the SWNTs are n-doped. The originality of this work lies in the complementarity between the microstructural characterizations, the electrical characterization and the theoretical calculations.

2. Material and methods

2.1. Synthesis of SWNTs

The SWNTs growth process is similar to that reported previously [21]. Briefly, the SWNTs were directly synthesized on SiO_2/Si substrates from thin evaporated Ru films (0.05 nm of Ru film thickness). The Ru catalyst was deposited on top of the substrates by ultra-high vacuum evaporation, similar to Molecular Beam Epitaxy (MBE). The SWNTs synthesis was

performed using a homemade double hot filament CVD (d-HFCVD) system. Prior to SWNTs growth, the substrates are heated at 850°C and exposed for 5 minutes to a hot-filament activated (160W – approximately 2000°C measured with an optical pyrometer) hydrogen flow (100 sccm at 90 mbar) to transform the Ru thin film into a random collection of Ru nanoclusters (dewetting operation). After this annealing under atomic hydrogen, a gas mixture CH_4:H_2 (1:5) is introduced into the reactor to grow SWNTs for 15 minutes. To efficiently pre-dissociate the CH_4 molecules, the methane flow is activated during SWNTs growth, by heating up the corresponding W filament at 1700°C (120 W). During growth, the hydrogen flow is also activated by heating up the corresponding filament at 2000°C (160 W - as for the dewetting of the Ru thin film). Thus, the generated atomic hydrogen is used to remove the undesired carbon nanoparticles and amorphous deposits formed on catalyst seeds and also on tube walls or substrate surface during d-HFCVD growth. During the heating, the substrate temperature was monitored by a pyrometer which can measure the sample temperature between 200 and 2000°C. We should note that the obtained SWNTs were used "as grown" and without any purification.

2.2. Functionalization of SWNTs

5,10,15,20-Tetraphenyl-21H,23H-porphine iron (III) chloride (Fe-Por), 5,10,15,20-Tetraphenyl-21H,23H-porphine cobalt(II) (Co-Por) and cobalt (II) phthalocyanin (Co-Phc) used in this work were purchased from "Sigma-Aldrich" France and used without any purification. The purity of Fe-Por, Co-Por and Co-Pc is 94%, 85% and 97%, respectively. All solvents: dichloromethane (DCM), N N-dimethylformamide (DMF) and acetone were purchased from "Sigma-Aldrich" France. The Fe-Por and Co-Por are very soluble in DCM and the Co-Phc is very soluble in DMF. The functionalization of SWNTs was achieved by the deposition of a solution of molecule (10 µl, 5.10^{-3} mol/l of Fe-Por or 10^{-4} mol/l Co-Por or 5.10^{-3} mol/l of Co-Phc) in DCM or DMF on the SWNTs surface followed by

evaporation/drying at 40°C for 1h. After rinsing several times with DCM or DMF to remove the excess of unbound molecules, the functionalized SWNTs (Fe-Por-SWNTs, Co-Por-SWNTs) or Co-Phc-SWNTs were then dried at 40°C for 5 min.

2.3. Characterization techniques

2.3.1. Raman spectroscopy. Raman spectra were recorded using a high-resolution confocal Raman microscope (Labram HR800; HORIBA Jobin Yvon France) through a 100× microscope objective (NA=1) in order to demonstrate the presence of porphyrin and phthalocyanine after functionalization. Micro-Raman mapping was performed in high resolution mode, using a laser excitation of λ=532 nm with 10 s acquisition time and 5 accumulations per spectrum. The number of gratings in the Raman spectrometer was 600 grooves per mm. Raman mapping was performed on 15 μm × 15 μm areas with a step size of 0.5 μm.

2.3.2. Scanning Electron Microscopy (SEM). SEM observations were carried out on a HITACHI S 4800 electron microscope. Further, to investigate the chemical state of the functionalized SWNTs, energy dispersive spectroscopy (EDS) analyses (Thermo Ultra Dry) have been performed.

2.3.3. Atomic Force Microscopy (AFM). AFM images were acquired using a VEECO Dimension 3100 instrument.

2.3.4. High Resolution-Transmission Electron Microscopy (HR-TEM) and Scanning Transmission Electron Microscopy (STEM). The HR-TEM analyses were performed using a FEI-Titan electron microscope operating at 80 and 300 kV. For the SWNTs (before and after functionalization) observations, an operating voltage of 80 kV was used in order to avoid any beam damage. Prior the TEM observations, a preliminary step was mandatory, consisting in transferring the SWNTs from the substrate surface onto Cu-mesh TEM grids. This has been done using a poly(methyl methacrylate) (PMMA) transfer method [22]. To protect the

SWNTs and facilitate their transfer, the PMMA was spin-coated on the Si/SiO_2-SWNTs at 3000 rpm for 40 s, followed by drying at 100°C for 5min. Then, the Si/SiO_2 was etched in NaOH (1mol/l) during 1h. The SWNTs/PMMA were recovered and placed into deionized (DI) water baths. After rinsing several times with DI water, the PMMA/SWNTs assembly was carefully deposited onto the TEM grid. Finally, the TEM grids were dried at 100°C during 24 h and then the PMMA was dissolved in acetone. The molecules (Fe-Por or Co-Por or Co-Phc) were deposited by evaporation of a 10 µL drop of a solution (Fe-Por or Co-Por or Co-Phc) in DCM or DMF directly on top of the surface of SWNTs followed by a thorough DCM or DMF washing process, to remove unbound molecules. Energy dispersive spectroscopy (EDS) elemental analyses at nanoscale resolution of functionalized SWNTs were performed on a 200 kV Titan-Themis TEM/STEM electron microscope equipped with a Cs probe corrector and a Chemistem Super-X detector. These two accessories allow chemical mapping of the light and heavy elements with a spatial resolution in the picometer range [23].

2.3.5. X-ray photoelectron spectroscopy (XPS). X-ray photoelectron spectroscopy (XPS) analysis was recorded using a Thermo Scientific K-Alpha spectrometer equipped with a micro-focused, monochromatic Al-Kα X-ray source (hν = 1486 eV) to give a spot size of 400 µm, and magnetic lens enables analysis of small areas with increased sensitivity. The operating pressure was around 2×10^{-9} Torr, and the kinetic energy of photoelectrons was determined with a hemispheric analyzer, with pass energies of 200 eV for survey spectra and 50 eV for high-energy resolution spectra. The charge neutralization was performed by a combination of an electron flood gun with an argon ion gun.

To check the reproducibility of the analysis, more than five samples were characterized for each functionalization. Different areas at the edge and the central region of samples were analyzed and typically showed similar characteristics.

2.3.6. Transport studies. The design of the CNTFETs used in this study has been described previously (see section V in supporting information) [21, 24]**.** Bottom-gate TFTs were fabricated by growing CNTs on SiO_2-silicon substrate. Following the nanotube growth, 40-nm thick source-drain palladium contacts were fabricated, using standard UV lithography, e-beam evaporation and lift-off processes. In this work, we used only the source-drain channel length (LSD) of 2-μm. The highly doped silicon substrate is used as a common back-gate for all transistors. The electrical characteristics of the CNTFETs were measured using a semiconductor parametric analyzer Keithley 4200-SCS under ambient conditions. The nanohybrid materials were produced by the evaporation of 10 μm drop of a solution of molecules (Fe-Por or Co-Por in DCM or Co-Phc in DMF) deposited directly on the CNTFETs surface. Followed by a drying step (1h at 40°C). The device was then thoroughly rinsed several times with DCM or DMF in order to remove unbound molecules.

3. Results and discussion

The resulting nanohybrid materials, denoted Fe-Por-SWNTs, Co-Por-SWNTs and Co-Phc-SWNTs, were first characterized by Raman spectroscopy to evidence the presence of an interaction between the molecules and SWNTs and also to ensure the efficiency of the assembly process. First, we focused our spectroscopic analysis on radial breathing modes (RBMs, between 100-300 cm^{-1}). It was previously reported that RBMs are very sensitive to the nanotube diameter and structure [25,26]. Figure 1 shows the Raman mapping at low frequency of SWNTs before and after functionalization with Fe-Por using an excitation wavelength of 532 nm (2.33 eV); the RBM spectra before and after functionalization with Co-Por and Co-Phc are presented in Figure S1 and S2 in Supporting Information. With excitation at 532 nm, multiple peaks are observed, which are characteristic of the distribution of tube diameters in the sample. Furthermore, the RBMs show some differences between the porphyrin-functionalized SWNTs and pristine (unfunctionalized) SWNTs (see Figure 1).

Indeed, the Raman spectrum of SWNTs shows four peaks at 150 cm^{-1}, 175 cm^{-1}, 248 cm^{-1} and 300 cm^{-1} in the RBM region. The Raman peak at 300 cm^{-1} can be assigned to the silicon substrate. In contrast, all bands were influenced by the functionalization of the SWNTs with porphyrin and additional bands were observed (Figure 1 (b)).

The Raman spectra at high frequency of pristine and functionalized SWNTs are presented in Figure 2. As shown in Figure 2 all Raman spectra revealed the presence of disorder-induced D-mode in the 1350 cm^{-1} region, Raman-allowed tangential G-band in the 1500-1600 cm^{-1} region and 2D-band in the 2700 cm^{-1} region [25-26]. Interestingly, the Raman spectra of resulting nanohybrid materials are significantly modified after the chemical functionalization process (Figure 2b, 2c and 2d). Indeed, additional bands (marked by a star in Fe-Por-SWNTs, an asterisk in Co-Por-SWNTs and an arrow in Co-Phc-SWNTs) that can be attributed to the presence of porphyrin and phthalocyanine are clearly discernable in the Raman spectra of functionalized SWNTs.

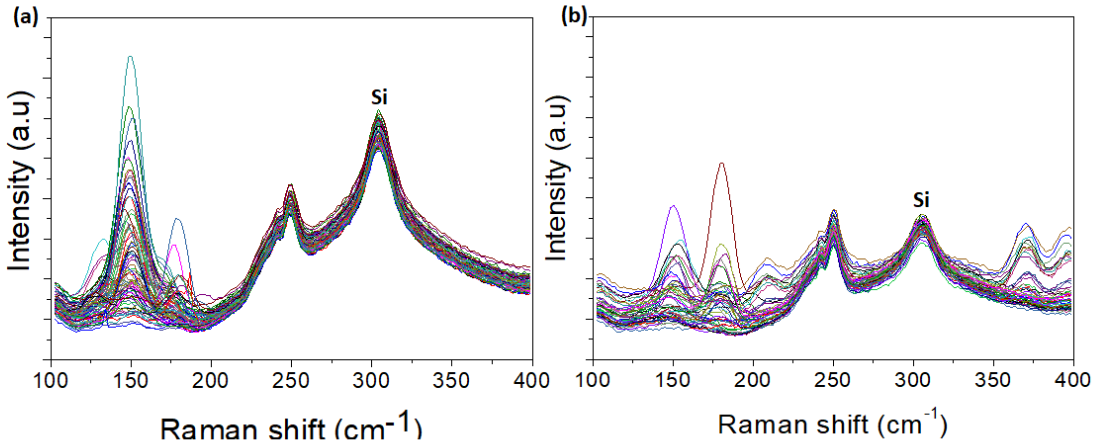

Figure 1. Raman radial breathing mode (RBM) of SWNTs before (a) and after functionalization with Fe-Por (b).

To confirm these results, an analytical blank silicon substrate surfaces functionalized with porphyrin and phthalocyanine were prepared and analyzed. It is important to note here that the silicon substrates were functionalized following the same process and then analyzed

with Raman spectroscopy. Figure S3 (a and b). shows the Raman mapping of functionalized silicon substrate with Fe-Por. The Raman spectra of functionalized silicon substrate with Co-Por and Co-Phc are presented in Figure S4 and S5 respectively in supporting information. The resulting bands (Figure S3) were found to be identical or close to additional bands observed previously in the case of Fe-Por-SWNTs, which confirm that these bands are characteristics of the Fe-Por. Similar results were obtained for Co-Por and Co-Phc (Figure S4 and Figure S5). We conclude that the spectra of functionalized SWNTs are roughly a combination of the spectra of their two subunits (i.e. individual SWNTs and porphyrin or phthalocyanine molecules). We should also note that the adsorption of porphyrin and phthalocyanine on the surface of SWNTs seems to be strong, as the molecules remain adsorbed despite extensive washing with organic solvent. Moreover, a shift of 1 to 3 cm^{-1} of all peaks after the functionalization process is also observed (see Figure 1 and Table 1). Similar shift was also observed for D and G bands.

Such upshift indicates an increase in energy and a stiffening of C-C bonds. This can also occur upon doping (see below, theory and electrical measurements) [27]. It was previously reported that charge transfer to and from SWNTs can alter C-C bonds in the nanotubes and thus the SWNT's electronic properties [28]. Further, metalloporphyrins are considered good electron donors that can give electrons to SWNTs, which would cause the characteristic shift of RBMs associated with an increase in electron density [29-30]. It was previously reported that such shift can also be attributed to the SWNTs organization within bundles and inter-nanotube contact [31]. However, we do not have bundles here. These Raman results constitute a first evidence of the successful non-covalent functionalization of our SWNTs.

Table 1. Raman shift on selected nanotubes presented in Figure 1 before and after functionalization with Fe-Por

Nanotube	RBM before functionalization (cm^{-1})	RBM after functionalization (cm^{-1})	Shift (cm^{-1})
Nanotube 1	248.294	250.1	+1.806
Nanotube 2	250.172	251.9	+1.728

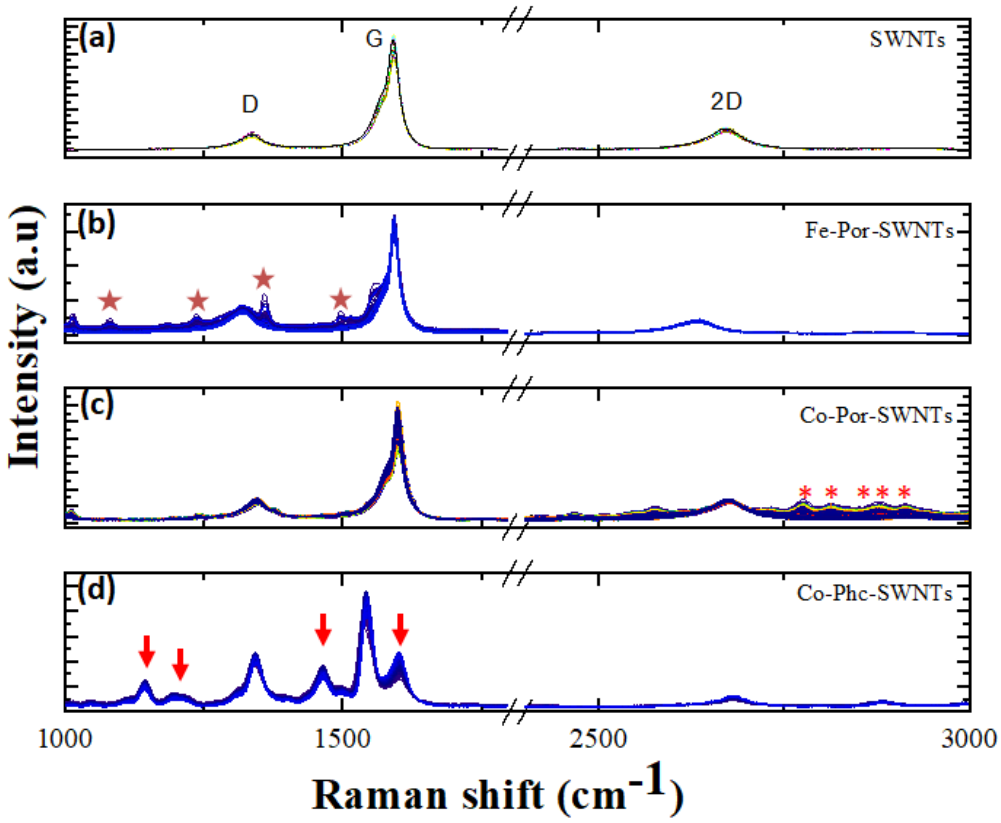

Figure 2. Raman spectra before and after functionalization showing the characteristic D, G and 2D peaks. (a): pristine SWNTs. (b): Fe-Por-SWNTs. (c) Co-Por-SWNTs and (d) Co-Phc-SWNTs. The additional bands marked by a star, an asterisk and an arrow are characteristics of Fe-Por, Co-Por and Co-Phc, respectively.

The assembly of porphyrin and phthalocyanine onto the SWNTs was further characterized by microscopy (SEM-EDX, AFM and TEM) methods. SEM images (inset Figure 3.) show that both samples have similar surface morphology, without any significant change after functionalization. To get more information on the presence of porphyrin and phthalocyanine molecules on the surface of SWNTs, EDS was used to identify elemental compositions. Figure 3 shows spectra obtained for EDS analyses performed on a large surface in SEM mode. The Fe and Co peaks in the EDS spectra (Figure 3(a), 3(b) and 3(c)) of the

corresponding SEM images (Figure 3(a) inset, 3(b) inset and 3(c) inset) indicate the existence of Fe, and Co within the field of the SEM image.

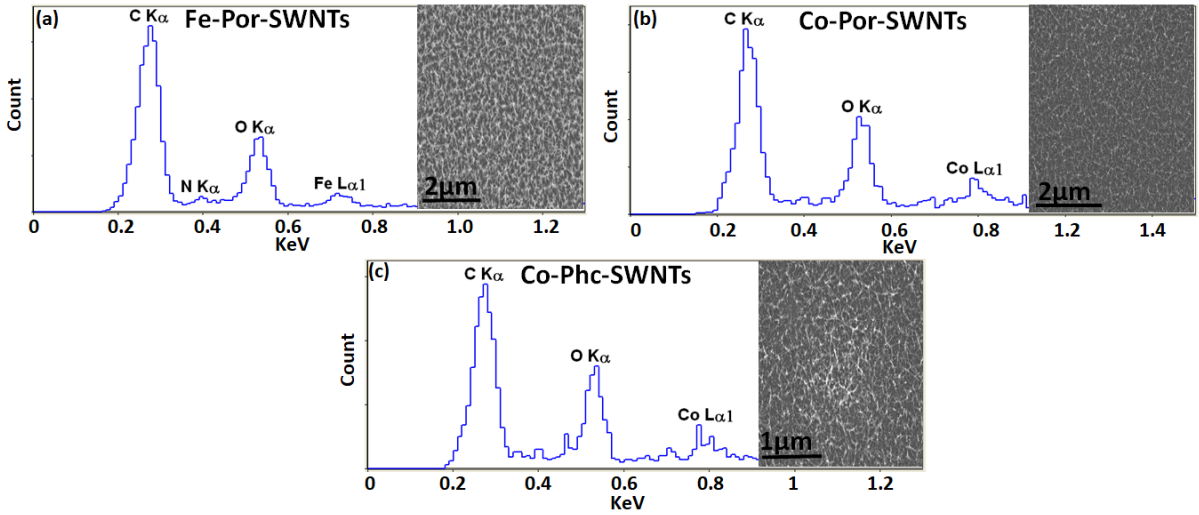

Figure 3. Energy-dispersive X-ray analysis (EDS) spectra and SEM images of functionalized SWNTs (inset). (a) Fe-Por, (b) Co-Por and (c) Co-Phc.

Complementary TEM and STEM investigations allowed a more detailed analysis of the nanohybrids. Figure 4(a, c and d) shows TEM images and Figure 4b a STEM-HAADF (high angle annular dark field) image recorded on a selection of representative functionalized samples with Fe-Por. Figure 4(a) shows pristine SWNTs, Figure 4(b) shows Fe-Por aggregates, Figure 4(c) shows SWNTs functionalized with Fe-Por, and Figure 4(d) is a zoom on a functionalized SWNT with Fe-Por. More TEM images of pristine SWNTs are shown in figure S6 in supporting information. TEM images of functionalized SWNTs with Co-Por-SWNTs and Co-Phc-SWNTs are presented in Figure S7 and S8 respectively in supporting information. As it can be seen in Figure 4(a) there is no amorphous carbon deposited on the outermost layers of SWNTs, however some defects and Ru nanoparticles are found (the Ru-nanoparticles originate from the SWNTs synthesis process). From the STEM-HAADF image represented in Figure 4(b) we can perceive small aggregates (4-8 nm) of Fe-Por before functionalization (the areas marked by the yellow arrows) and also the presence of very few aggregates on the surface of SWNT (70-90 nm), which can be related to different interaction

behavior with carbon support. We should note at this point that the same procedure was applied for the functionalization of grids TEM to obtain TEM images. Image of functionalized SWNTs reveals the presence of overcoating on the sidewalls of the surface of the tubes (Figure 4(c)) when compared with the pristine one. These overcoatings are observed on almost all individual tubes. These features are clearly a result of functionalization, but we cannot derive much information concerning the homogeneity of the functionalization of the nanotubes. Similar results were obtained for Co-Por-SWNTs and Co-Phc-SWNTs see Figure S7 and Figure S8 in supporting information. Moreover, the TEM images does not show any aggregates of molecules.

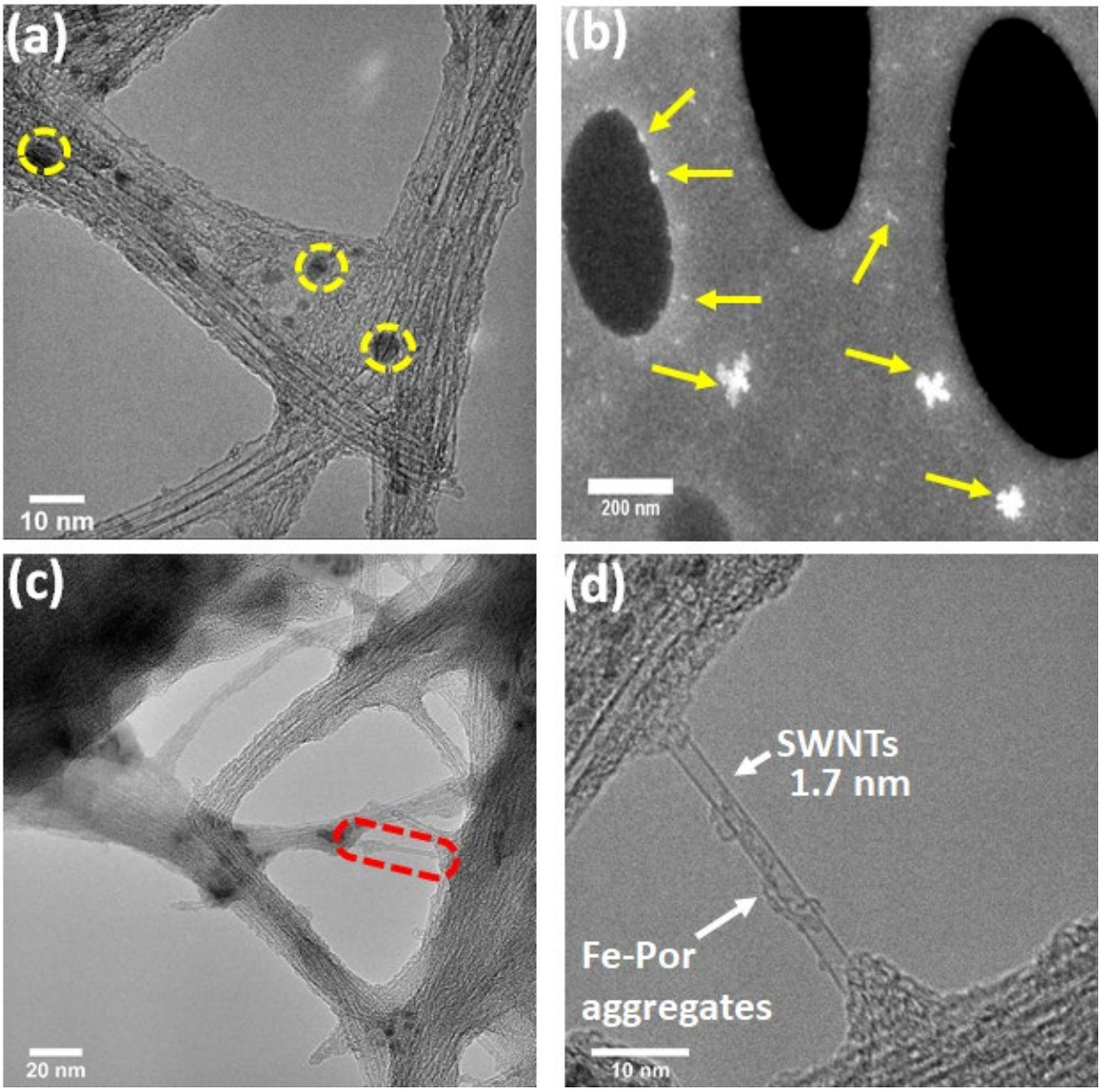

Figure 4. TEM and STEM observations of SWNTs functionalized with Fe-Por. (a) Pristine SWNTs synthesized from a 0.05 nm-thick Ru layer at 850°C under atomic hydrogen flux (H_{at}). (b) STEM-HAADF image of Fe-Por. (c) HR-TEM image of functionalized SWNTs with Fe-Por. (d) HR-TEM image zoom of the area marked by the red dotted rectangle in (c) showing one functionalized SWNT with Fe-Por aggregates.

To prove the physi-adsorption of molecules on individual SWNTs, without decomposition, we performed chemical analyses in scanning transmission electron microscopy- high angle annular dark field- energy dispersive X-ray spectroscopy (STEM-HAADF-EDS) mode. Figure 5 shows STEM-EDS line scan analyses on an individual SWNT

functionalized with Fe-Por. Others areas on the surface of substrate are presented in Figure S9. Figure S10 and Figure S11 in supporting information show STEM-HAADF chemical maps corresponding to the Co-Por and Co-Phc together with their corresponding Co/N/C relative maps obtained by superimposing the three elemental maps. This provides a complete image of the distribution of the two principal residual elements, Co and N, within the sample. Elemental maps were extracted at energies of 6.92 keV (Co Kα). The light elemental content within the sample was also confirmed by the line scan EDS spectrum recorded along the scanning direction indicated by the yellow arrow in Figure 5 (a). Indeed, from Figure 5(b) one can identify the elemental signal of N, Fe and Cl, which are characteristics of Fe-Por. The Ru signal was also detected and it originates from the catalysts used for the synthesis of SWNTs.

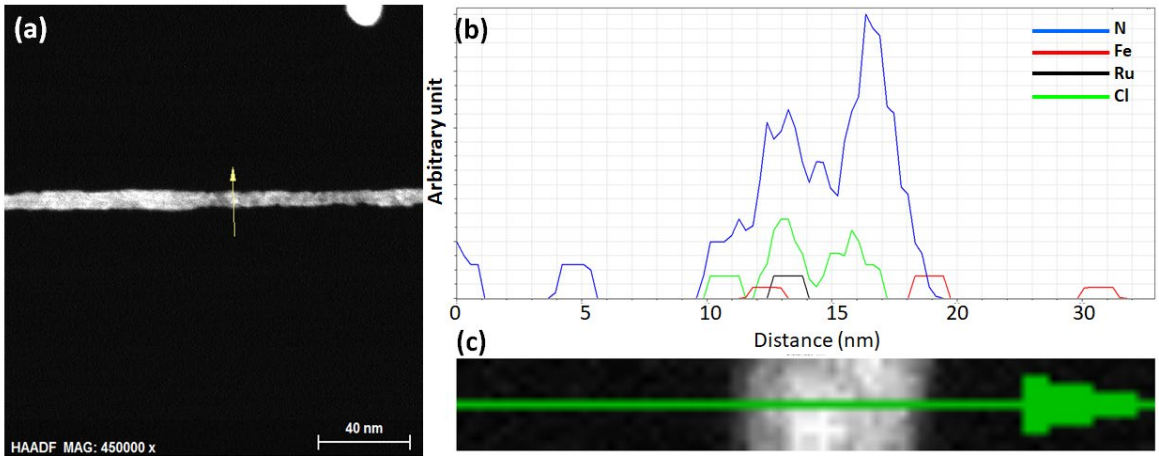

Figure 5. STEM-EDS line scan analyses on an individual functionalized SWNTs: **(a)** STEM-HAADF micrograph on the chosen area where a line scan along the direction indicated by the green arrow was performed. (**b**) Corresponding STEM-EDS line scan spectrum showing the variation of the Nitrogen (in blue), Iron (in red), Ruthenium (in black) and Chlorine (in green) signal recorded along the scanning direction indicated by the green arrow in (c). (c) Zoom of the analyzed area indicated by yellow arrow in (a).

Additionally to this study, Figure S12 in supporting information shows the STEM-HAADF-EDS relative map recorded on a larger area, obtained by superimposing the elemental maps recorded for the carbon, silicon, iron, chlorine and the oxygen where the nitrogen signal is slightly visible. These results confirm that the chemical integrity of porphyrin and phthalocyanine remained intact in the nano-hybrids, which is in good agreement with Raman spectroscopy and SEM-EDS analysis and suggests that the porphyrin

and phthalocyanine strongly interact with π-system of SWNTs due to their highly-delocalized π-system.

The successful adsorption of porphyrin and phthalocyanine was also confirmed by atomic force microscope (AFM) investigations. A detailed analysis of the AFM profiles on a large number of tubes allowed us to assess that the diameter of all synthetized tubes is about 1.5 nm with a standard deviation of about 0.5 nm (see Figure 6). However, the diameter of SWNTs functionalized with porphyrin and phthalocyanine is significantly higher (2 to 7 nm) than the average diameter of individual SWNTs. The height difference between the functionalized SWNTs and the individual SWNTs is about 0.5 to 5.5 nm, which is larger than the diameter of a porphyrin or phthalocyanine molecule (0.3 to 1 nm). As observed in Figure 4 (d), the Fe-Por "wraps" the SWNTs or is attached to both sides of a single nanotube, which explains the increases of the diameter of SWNTs after functionalization.

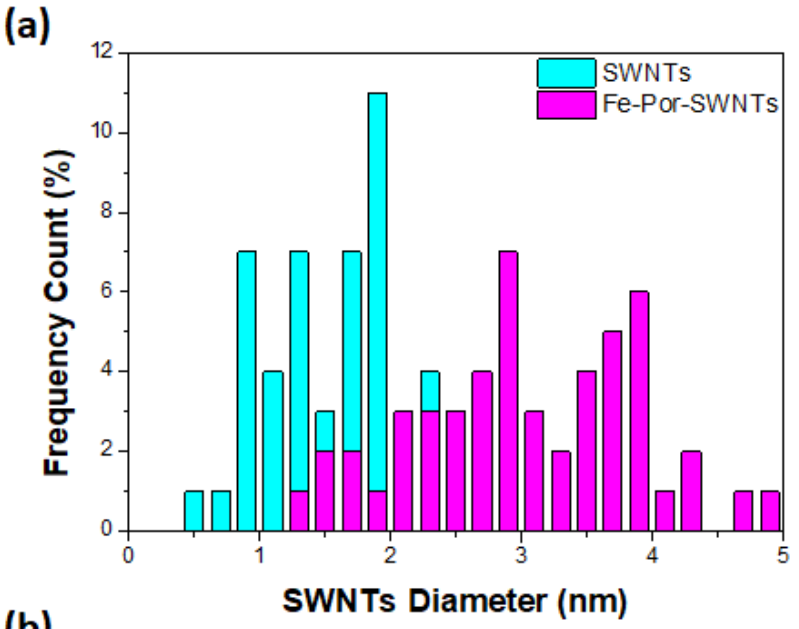
(a)
SWNTs
Fe-Por-SWNTs
Frequency Count (%)
SWNTs Diameter (nm)

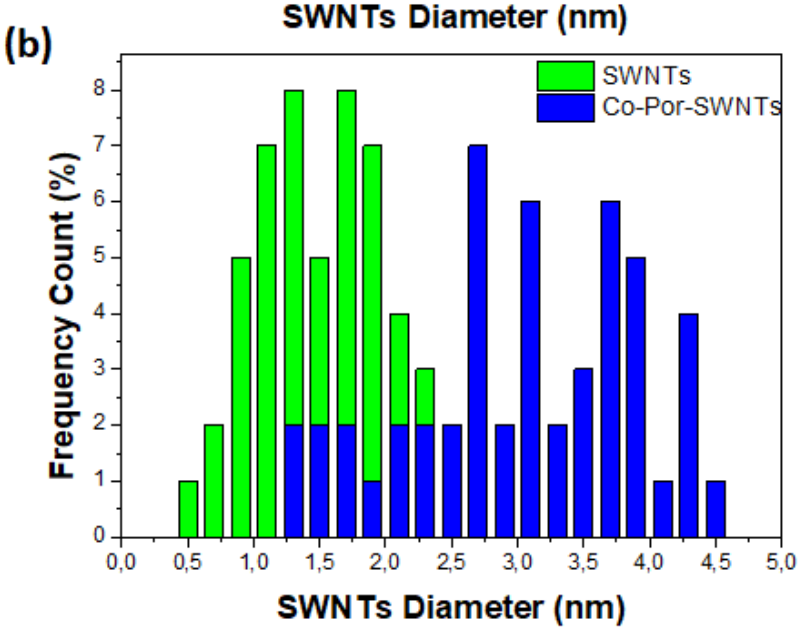
(b)
SWNTs
Co-Por-SWNTs
Frequency Count (%)
SWNTs Diameter (nm)

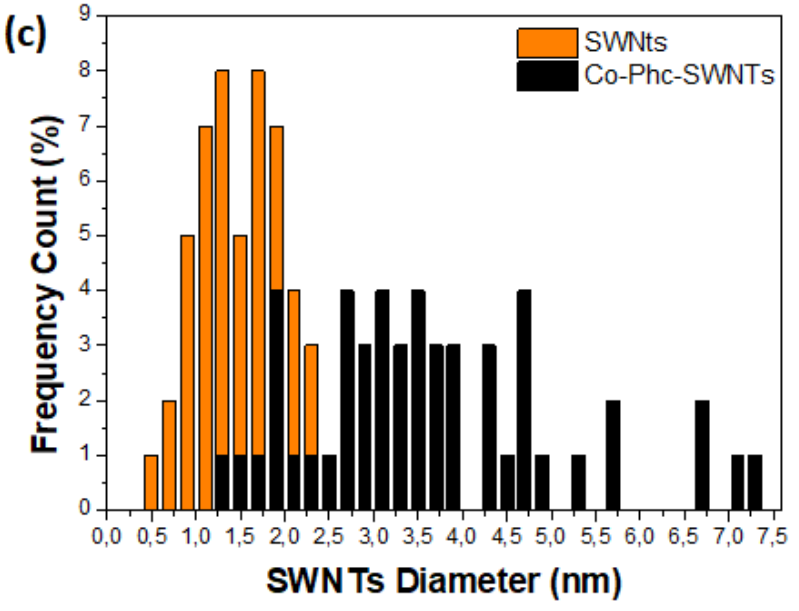
(c)
SWNts
Co-Phc-SWNTs
Frequency Count (%)
SWNTs Diameter (nm)

Figure 6. Column stack diameter distribution of the SWNTs before and after functionalization obtained from 20 AFM height images. (a) Fe-Por, (b) Co-Por and (c) Co-Phc.

From all the above studies, we confirm that the porphyrin and phthalocyanine assemble well onto nanotube sidewalls. These results are consistent with those from the literature, which reported that porphyrin and phthalocyanines strongly interact with the π-electronic surface of SWNTs [16, 17]. Murakami *et al.* have successfully modified SWNTs by attaching Zn-porphyrin through non-covalent functionalization [16]. A similar approach has also been reported by Rahman *et al.* [17].

Further characterization of SWNTs before and after the functionalization with Co-porphyrins and Co-phtalocyanine was carried out by X-ray photoelectron spectroscopy. The XPS spectra displayed in Figure 7 revealed obvious modifications after functionalization of SWNTs confirming the presence of metalloporphyrin and metallophthalocyanine at the surface of SWNTs. It can be seen from Figure 7a that all the survey spectra show peaks centered at 100, 150, 284, 530 eV respectively assigned to Si2s, Si2p, C1s, and O1s originated from SiO_2/Si substrates and SWNTs. In addition, one can clearly detect from the spectra of functionalized SWNTs the appearance of peaks centered at 400 eV and 785 eV assigned to N1 and Co2p, respectively (Figure 7b and 7c). This is due to the adsorption of cobalt porphyrin and cobalt phthalocyanine on the SWNTs. As shown in Figure 7d, the C1s spectrum of pristine SWNTs can be deconvoluted into four main components centered at 284.6, 286.7, 288.5, and 290.5 eV corresponding to C=C/C-C/C-H, C-O-C/C-OH, OH-C=O bonds, and π–π* shakeup satellites in aromatic rings, respectively. The broadening of the C1s spectra of functionalized SWNTs at around 286 eV indicates the presence of C-N as well as C=N components, owing to the interaction between Co-Por and Co-Phc molecules with SWNTs (Figure 7e and 7h) [32].

The N1s high-resolution spectra recorded from Co-Por-SWNTs and Co-Phc-SWNTs confirm these results which show that the components are N=C, N-C/N-Co, and $^{+}NR_4$ located around 398.8, 400.2 and 402 eV, respectively (Figure 7f and 7i). Co2p spectra (Figure 7g and 7j) can be deconvoluted into five main component peaks, including $Co2p_{3/2}$ signals at 781.5 eV, $Co2p_{3/2}$ satellite at 786.5 eV, $Co2p_{1/2}$ signals at 797 eV and $Co2p_{3/2}$ satellite at 804 eV associated to Co(II) ions and an additional component at 791 eV assigned to the oxidized state of cobalt, i.e. Co(III). The presence of Co (III) is due to the fact that cobalt can be easily oxidized when exposed to air. These XPS results are in good agreement with those shown with Raman and HRTEM analyses.

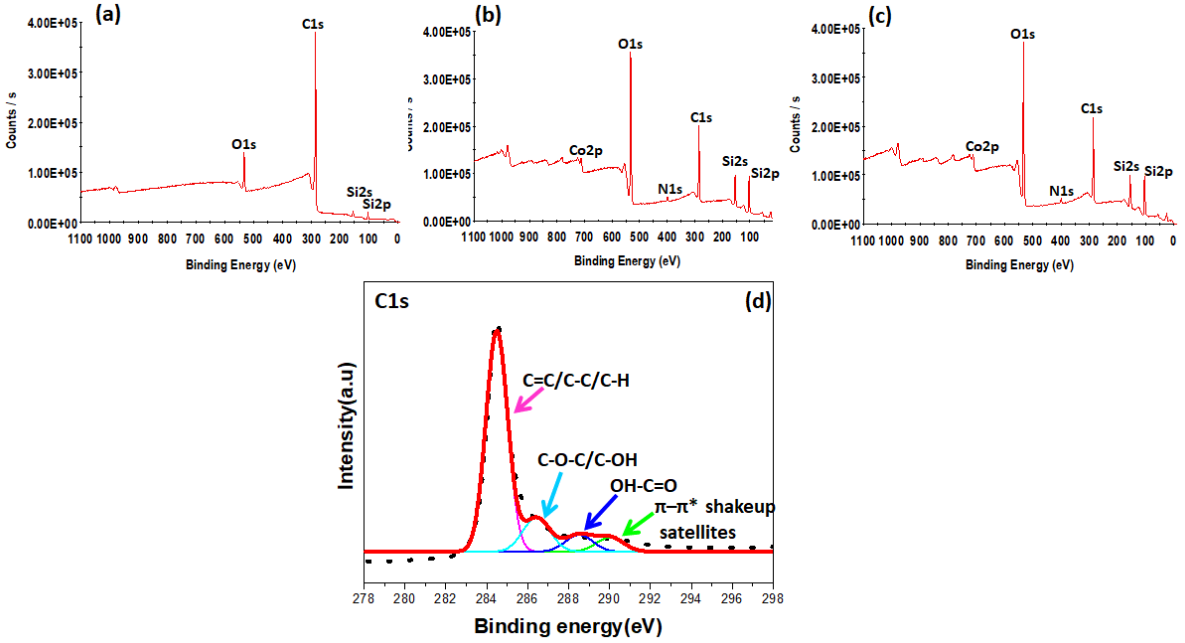

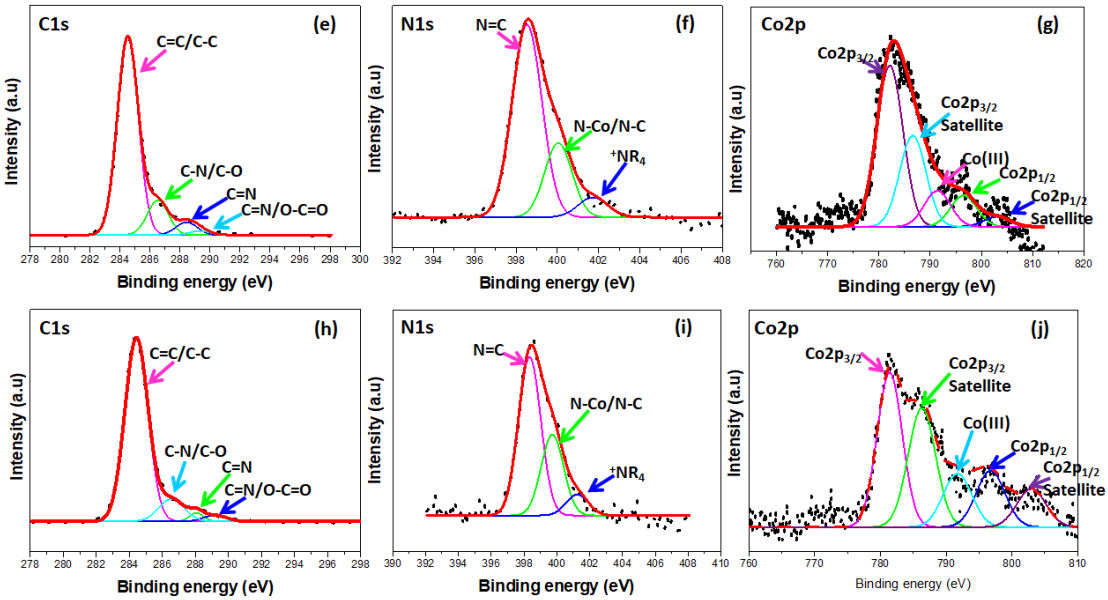

Figure 7. (a-c) XPS spectra of SWNTs and functionalized SWNT (Co-Por-SWNTs and Co-Phc-SWNTs); the spectra show the presence of silicon, carbon and oxygen in SWNTs and additional peaks corresponding to the presence of nitrogen and cobalt coming from porphyrin in functionalized SWNTs (Co-Por-SWNTs and Co-Phc-SWNTs). (e-j) Deconvoluted core level XPS spectra of the principal elements (i.e. C 1s, N1s and Co2p) of Co-Phc-SWNTs (e-g) and Co-Por-SWNTs (h-j).

To rationalize the molecule−SWNTs interactions, theoretical density functional theory calculations (DFT) (open shell) were carried out using CRYSTAL17 code [33] (The computational details are provided in supporting information). In this study, we focus only on a semiconductor nanotube to compare the theoretical results with the electrical measurements. For computational conveniences, SWNT (8,0) has been chosen. The SWNT (8,0) has an atomic structure called a zigzag (SWNT (n,0)) [34]. The diameter of SWNT (8,0) equals $8a/\pi$ = 0.63 nm (a = 0.249 nm = the module of the unit vectors of the graphene lattice) such that it is a reasonable compromise between computation costs and a realistic size. Moreover SWNT (8,0) has been widely studied and the theoretical calculation results can be found in the literature [35-39]. For the optimized geometry of the SWNT (8,0), the PBE0 calculated band gap is 1.55 eV. The PBE0 functional value is in better agreement with the experimental one of 1.99 eV [40], compared with values obtained by other functionals such as B3LYP or PBE,

their corresponding calculated band gap values being 1.28 eV [38] and 0.58 eV [39], respectively.

Figure 8.1 shows the most stable geometry of SWNT (8,0) grafted by Co-porphyrin. The binding energies (E_b in kJ/mol) is calculated at -125.74 kJ/mol, in agreement with previous work [41] (see supporting information for the details of calculations and results in Table S1).

At the respective equilibrium geometries, the metal center (cobalt (II)) of the Co-Por molecule is on the top of a SWNT (8,0) hexagon center (see Figure 8.1). The fermi levels of SWNT (8,0) and Co-Por on SWNT (8,0) are presented in Figure 8.2. The charge transfer is of 0.04953e from the Co-Por towards SWNT (8,0). The theoretical results indicate that the Fermi level increases with the adsorption of the porphyrin molecule on the surface of the SWNT, confirming that the molecule is electron donor. The semiconductor SWNT (8,0) is then n-doped by the porphyrin molecule. This result is in a good agreement with the experimental results (see electrical results in the section below).

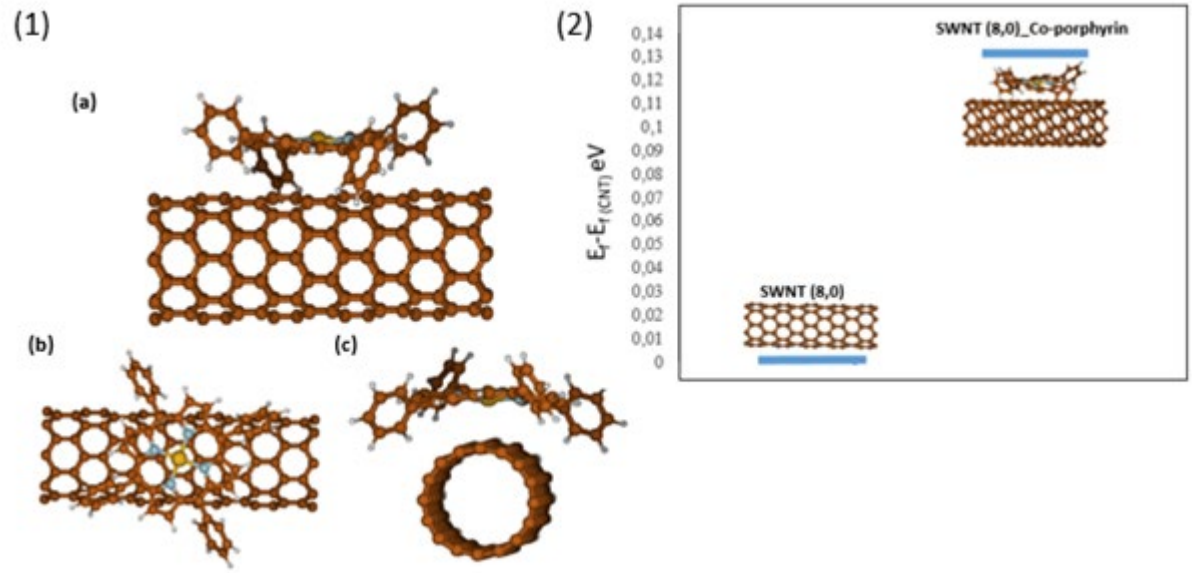

Figure 8. (1). Optimized geometry of the Co-Por adsorbed on the SWNT (8,0). (a) front view, (b) top view and (c) side view. (2). Fermi levels of SWNT (8,0) and SWNT (8,0)_Co-Por at the PBE0-D3/6-31G** level of theory using CRYSTAL.

To get more insights on the electronic interaction occurring between the compounds and SWNTs and to confirm the charge transfer, we studied the transport behavior using CNTFET devices in ambient air. The devices were obtained following the previously reported method [21,24]. Briefly, the interdigitated electrodes made of Pd (40 nm) were deposited onto SWNTs directly on SiO_2/Si substrate. As already stated in our previous reports [21, 24], we not that the presence of the Ru catalyst does not reduce the devices performance. Typical transfer characteristics of such bottom gate devices before functionalization (with channel length and width of respectively L= 2μm and W = 2 mm) are displayed in Figure 10 (black curve). The electrical characteristics of CNTFETs before functionalization exhibits typical p-type response with "on" and "off" current (I_{on}/I_{off}) ratio of about four decades. The hysteresis is also observed as a result of charge injection from the SWNTs to the SiO_2 [42].

Such CNTFETs devices present high performance, comparable to CNTFETs devices based on individual semiconducting SWNTs, which make them more suitable for detecting even the slightest change in the transport properties of SWNTs. The transport studies were carried out using the functionalized CNTFET devices in ambient air with a drain bias (V_d) of 2V and a gate voltage (V_g) sweep [-20 V; +20 V]. The SEM images of CNTFET device after functionalization with Fe-porphyrin are presented in Figure S14 in supporting information. The carrier mobility calculated for those devices is about 10-15 cm^2/Vs as evaluated by the standard MOS formula [43] (see paragraph V in supporting information). We note that the mobility value we obtain here is quite modest; we suspect some contact problems in our FETs. Figure 9 shows the drain current (I_{ds}) vs. gate voltage (V_g) characteristics of functionalized CNTFETs with Fe-Por. The I_{ds} vs. V_g characteristics of functionalized CNTFETs with Co-Por-SWNTs and Co-Phc-SWNTs are presented in Figure S15 and S16 in supporting information. The subthreshold swing Sw = [dVg/d Log(I)] remains unchanged after functionalization with Fe-Por, indicating that such grafting leaves the gate (Si)

unaffected. In contrast, the I_{on} slightly decreases, which confirm that the grafted molecule perturb the electron flow, producing scattering centers [44]. Furthermore, some changes were observed on the I_{ds} vs. V_g hysteresis curves after the functionalization. A 300 meV threshold voltage shift is observed after functionalization, the gate voltage V_{th} shifts to negative values, from -5.08 V to -8.39 V. This shift, evidences that Fe-Por interacts with the nanotube sidewalls and confirms a "n" type doping of the CNTs. This behavior has been observed for a series of 20 devices with the same channel length and prepared under the same conditions (see Figure S15 in supporting information). This is in agreement with previous reports stating that the metalloporphyrins are good electron donors [45] that can give electrons to SWNTs [29-30, 45], which would cause an increase of the electronic density. Similar results are obtained for Co-Por and Co-Phc (see Figure S16 and S17 in supporting information). The electrical measurements confirm the theoretical one, particularly the raise of the Fermi level due to doping.

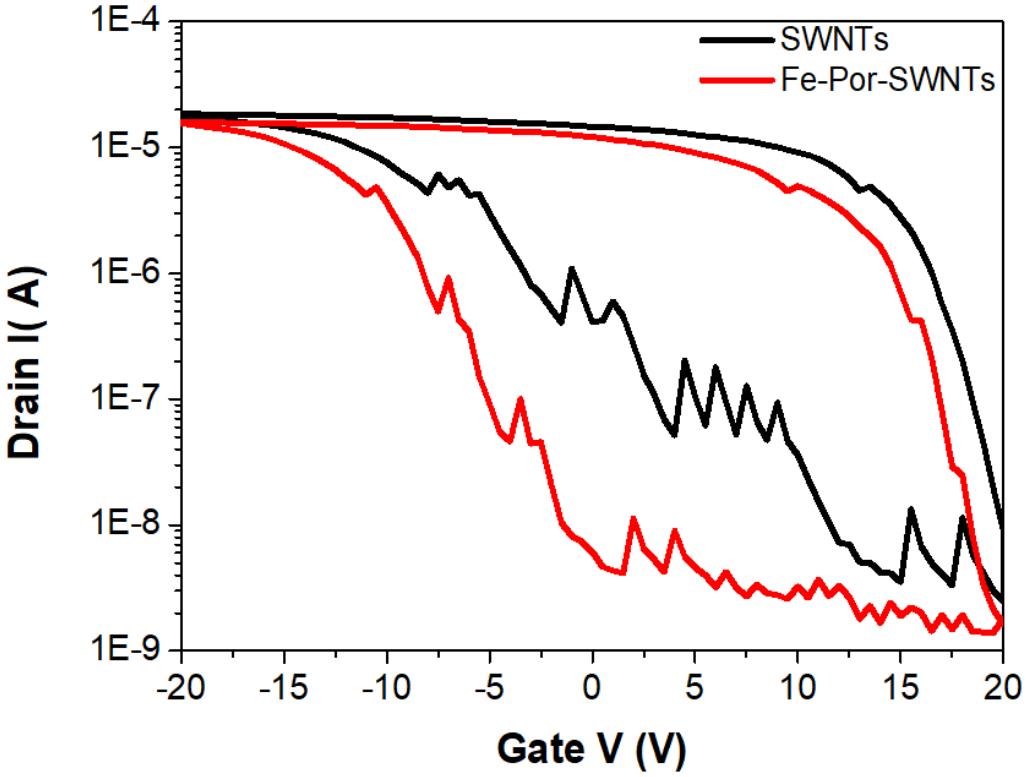

Figure 9. I_{ds} vs V_g characteristics for a) CNFET (black) and the same CNTFET modified with Fe-Por (red). V_{ds} = 2V.

4. Conclusion

In summary stable Fe-SWNTs, Co-Por-SWNTs and Co-Phc-SWNTs nano-hybrids materials have been elaborated. A series of microscopic, spectroscopic and electrical analyses reveals that these systems interact non-covalently via π-stacking, which are more likely to preserve the SWNTs electronic properties. One of the consequences of π-stacking interactions is charge transfer between the metal-centered molecules and the SWNTs. Electrical measurements performed on CNTFETs are in a good agreement with the theoretical ones, which confirm the n-type doping effect (electron transfer) of SWNTs when the MPo and MPc molecules are grafted. Taking into account the robustness and the scalability of the functionalization approach, we believe that these results are extremely promising for the future development of CNTs-based selective gas sensing applications.

Author Contributions

F. Bouanis, A. Yassar, C.Leonard and D. Pribat planned and conceived the experiments and studies. F.B. prepared and characterized the surface by Raman, AFM and SEM-EDX. F.B and I.Florea prepared and performed the HR-TEM-STEM studies. F.B, S.M-C. B.C. and D.G

prepared and performed XPS studies. F.B. designed, prepared the devices and performed the transport studies. C.L and M.B. carried out the theoretical studies. All authors contributed to the analysis of the different studies. F.B, A.Y., C.L. and D.P. wrote the paper with contributions from all the authors.

Acknowledgements: This work was carried out with partial support from I-Site Future in the framework of the project "Capteur". The authors acknowledge financial support from the French state managed by the National Research Agency under the Investments for the Future program under the references ANR-10-EQPX-50. Part of the TEM analysis has been carried out at Centre Interdisciplinaire de Microscopie électronique de l'X (CIMEX) which is gratefully acknowledged.

Supporting Information. Brief descriptions in nonsentence format listing the contents of the files supplied as Supporting Information.

References:

[1] P. J. F. Harris, Carbon Nanotubes and Related Structures: New Materials for the Twenty-First Century; Cambridge University Press: Cambridge, UK, 2001.

[2] J. Kong, N. R. Franklin, C. Zhou, M. G. Chapline, S. Peng, K. Cho, H. Dai, Nanotube Molecular Wires as Chemical Sensors Science 287 (2000) 622-625. DOI: 10.1126/science.287.5453.622

[3] M. S. Dresselhaus, G. Dresselhaus, Ph. Avouris, Eds. Carbon Nanotubes: Synthesis, Structure and Applications; Springer Publishing: New York, 2001.

[4] T. Zhang, S. Mubeen, E. Bekyarova, B. Y. Yoo, R. C. Haddon, N. V. Myung, M. A. Deshusses, Poly(m-aminobenzene sulfonic acid) functionalized single-walled carbon nanotubes based gas sensor, Nanotechnology 18 (2007) 165504. DOI: 10.1088/0957-4484/18/16/165504

[5] M. Zhu, J. Chen, L. Huang, R. Ye, J. Xu, Y. F. Han, Covalently Grafting Cobalt Porphyrin onto Carbon Nanotubes for Efficient CO_2 Electroreduction, Angew. Chem. Int. Ed. 58 (2019) 1-6. https://doi.org/10.1002/anie.201900499

[6] V. Sgobba, D. M. Guldi, Carbon nanotubes—electronic/electrochemical properties and application for nanoelectronics and photonics, Chem. Soc. Rev. 38 (2009) 165. https://doi.org/10.1039/B802652C

[7] W. Yang, P. Thordarson, J. J. Gooding, S.P. Ringer, F. Braet, Carbon nanotubes for biological and biomedical applications, Nanotechnology 18 (2007) 412001. DOI: 10.1088/0957-4484/18/41/412001

[8] M. Biesaga, K. Pyrzynska, M. Trojanowicz, Porphyrins in analytical chemistry: A review. 51 (2000) 209-224. https://doi.org/10.1016/S0039-9140(99)00291-X

[9] M. Ethirajan, Y. Chen, P. Joshi, R. K. Pandey, The role of porphyrin chemistry in tumor imaging and photodynamic therapy, Chem. Soc. Rev. 40 (2011) 340 –362. DOI: 10.1039/b915149b

[10] A. Merhi, S. Drouet, N. Kerisit, C. O. Paul-Roth, A Family of Fluorenyl Dendrons For Porphyrin Dendrimers synthesis, Tetrahedron 68 (2012) 7901 –7910. DOI : 10.1016/j.tet.2012.07.018

[11] T. Palacin, H. L. Khanh, B. Jousselme, P. Jegou, A. Filoramo, C. Ehli, D. M. Guldi, S. Campidelli, Efficient functionalization of carbon nanotubes with porphyrin dendrons via click chemistry, J. Am. Chem. Soc. 131 (2009) 15394-15402. https://doi.org/10.1021/ja906020e

[12] S. Campidelli, B. Ballesteros,A. Filoramo, D. Dı´az-Dı´az, G. de la Torre, T. Torres, G. M. A. Rahman, C. Ehli, D. Kiessling, F. Werner, V. Sgobba, D. M. Guldi, C. Cioffi, M. Prato and J.-P. Bourgoin, Facile Decoration of Functionalized Single-Wall Carbon Nanotubes with

Phthalocyanines via “Click Chemistry”, J. Am. Chem. Soc., 130 (2008) 11503-11509. https://doi.org/10.1021/ja8033262

[13] A. Şenocak, E. Demirbaş, M. Durmuş, Phthalocyanine-Nanocarbon Materials and Their Composites: Preparation, Properties, and Applications. In: Nanocarbon and Its Composites (Khan A., Jawaid M., Asiri I.A., Eds.), Elsevier, (2019) 677–709. doi:10.1016/B978-0-08-102509-3.00023-7.

[14] Y. Zhou, Y. Fang, R. P. Ramasamy, Non-Covalent Functionalization of Carbon Nanotubes for Electrochemical Biosensor Development, Sensors 19 (2019) 392. doi:10.3390/s19020392.

[15] V. Sgobba, G. M. A. Rahman, C. Ehli, D. M. Guldi, Covalent and Non-covalent Approaches Toward Multifunctional Carbon Nanotubes Materials In Fullerenes-Principles and Applications, Eds. Royal Society of Chemistry: Cambridge, UK, 2007.

[16] H. Murakami, T. Nomura and N. Nakashima, Noncovalent porphyrin-functionalized single-walled carbon nanotubes in solution and the formation of porphyrin-nanotube nanocomposites, Chem. Phys. Lett., 378 (2003) 481-485. https://doi.org/10.1016/S0009-2614(03)01329-0

[17] H. Li, S. I. Song, G. Y. Song, I. Kim, Non-covalently functionalized carbon nanostructures for synthesizing carbon-based hybrid nanomaterials, J. Nanosci. Nanotechnol., 14 (2014) 1425–1440. doi:10.1166/jnn.2014.9048**.**

[18] G. Speranza, The Role of Functionalization in the Applications of Carbon Materials: An Overview, J-C. Carbon Res., 5 (2019) 84. doi:10.3390/c5040084.

[19] F. Cheng, A. Adronov, Suzuki Coupling Reactions for the Surface Functionalization of Single-Walled Carbon Nanotubes, Chem. Mater. 18 (2006) 5389-5391. https://doi.org/10.1021/cm061736j

[20] J.K. Sprafke, S.D. Stranks, J.H. Warner, R.J. Nicholas, H.L. Anderson, Noncovalent Binding of Carbon Nanotubes by Porphyrin Oligomers, Angew. Chem. 123 (2011) 2361 – 2364. https://doi.org/10.1002/anie.201007295

[21] F.Z. Bouanis, I. Florea, M. Bouanis, D. Muller, A. Nyassi, F. Le Normand, D. Pribat, Diameter controlled growth of SWCNTs using Ru as catalyst precursors coupled with atomic hydrogen treatment, Chemical Engineering Journal 332 (2018) 92-101. https://doi.org/10.1016/j.cej.2017.09.073

[22] L. Jiao, B. Fan, X. Xian, Z. Wu, J. Zhang, Z. Liu, Creation of Nanostructures with Poly(methylmethacrylate)-Mediated Nanotransfer Printing, J. Am. Chem. Soc. 130 (2008) 12612–12613. https://doi.org/10.1021/ja805070b

[23] L. Loisel, I. Florea, C. S. Cojocaru, B. Kang Tay, B. Lebental, Oxidation-based continuous laser writing in vertical nano-crystalline graphite thin films, Sci. Rep. 6 (2016) 26224. DOI : 10.1038/srep26224

[24] F.Z. Bouanis, C.S. Cojocaru, V. Huc, E. Norman, M. Chaigneau, J.L. Maurice, T. Mallah, D. Pribat, Direct Synthesis and Integration of Individual, Diameter-Controlled Single-Walled Nanotubes (SWNTs), Chem. Mater. 26 (17) (2014) 5074-5082. https://doi.org/10.1021/cm502282x

[25] M. S. Dresselhaus, G. Dresselhaus, A. Jorio, A. G. Souza Filho, M. A. Pimenta, R. Saito, Single nanotube Raman spectroscopy, Acc. Chem. Res. 35 (2002) 1070-1078. https://doi.org/10.1021/ar0101537

[26] M. S. Dresselhaus, G. Dresselhaus, A. Jorio, A. G. Souza Filho, R. Saito, Raman spectroscopy on isolated single wall carbon nanotubes, Carbon 40 (2002) 2043-2061. https://doi.org/10.1016/S0008-6223(02)00066-0

[27] V. Ska´kalova´, A. B. Kaiser, U. Dettlaff-Weglikowska, K. Hrncarikova, S. Roth, Effect of Chemical Treatment on Electrical Conductivity, Infrared Absorption, and Raman Spectra of Single-Walled Carbon Nanotubes, J. Phys. Chem. B, 109 (15) (2005) 7174-7181. https://doi.org/10.1021/jp044741o

[28] D.A. Britz, A. N. Khlobystov, Noncovalent interactions of molecules with single walled carbon nanotubes, Chem. Soc. Rev., 35 (2006) 637–659. https://doi.org/10.1039/B507451G

[29] D. M. Guldi, H. Taieb, G. M. A. Rahman, N. Tagmatarchis, M. Prato, Novel Photoactive Single-Walled Carbon Nanotube–Porphyrin Polymer Wraps: Efficient and Long-Lived Intracomplex Charge Separation, Adv. Mater., 17(7) (2005) 871-875. https://doi.org/10.1002/adma.200400641

[30] D. M. Guldi, G. M. A. Rahman, N. Jux, N. Tagmatarchis, M. Prato, Integrating single-wall carbon nanotubes into donor-acceptor nanohybrids, Angew. Chem., Int. Ed., 43 (2004) 5526-5530. doi: 10.1002/anie.200461217

[31] D. A. Heller, P. W. Barone, J. P. Swanson, R. M. Mayrhofer, M. S. Strano, Using Raman Spectroscopy to Elucidate the Aggregation State of Single-Walled Carbon Nanotubes, J. *Phys. Chem. B 108 (*2004) 6905-6909. https://doi.org/10.1021/jp037690o

[32] G. Polzonetti, C. Battocchio, A. Goldoni, R. Larciprete, V. Carravetta, R. Paolesse, M. V. Russo, Interface formation between C_{60} and diethynyl-Zn-porphyrinato investigated by

SR-induced photoelectron and near-edge X-ray absorption (NEXAFS) spectroscopies, Chem. Phys. 297 (2004) 307-314. https://doi.org/10.1016/j.chemphys.2003.10.024

[33] R. Dovesi, A. Erba, R. Orlando, C. M. Zicovich-Wilson, B. Civalleri, L. Maschio, M. Rerat, S. Casassa, J. Baima, S. Salustro, B. Kirtman. Quantum-mechanical condensed matter simulations with CRYSTAL, WIREs Comput Mol Sci. 8 (2018) e1360. https://doi.org/10.1002/wcms.1360

[34] A. Krüger, Neue Kohlenstoffmaterialien - Eine Einführung. Teubner (2007) 125−286.

[35] C.R. Luna, P. Bechthold, G. Brizuela, A. Juan, and C. Pistonesi, The adsorption of CO, O_2 and H_2 on Li–doped defective (8,0) SWCNT: A DFT study, App. Surf. Sci., 459 (2018) 201–207. https://doi.org/10.1016/j.apsusc.2018.07.171

[36] V. Verdinelli, E. German, C. R. Luna, J. M. Marchetti, M. A. Volpe, and A. Juan, Theoretical Study of Hydrogen Adsorption on Ru-Decorated (8,0) Single-Walled Carbon Nanotube, J. Phys. Chem. C, 118 (2014) 27672−27680. https://doi.org/10.1021/jp508183t

[37] H. Valencia, A. Gil, and G. Frapper, Trends in the Adsorption of 3d Transition Metal Atoms onto Graphene and Nanotube Surfaces: A DFT Study and Molecular Orbital Analysis, J. Phys. Chem. C, 114 (2010) 14141–14153. https://doi.org/10.1021/jp103445v

[38] Y. Matsuda, J. Tahir-Kheli, and W. A. Goddard, Definitive band gaps for single-wall carbon nanotubes, J. Phys. Chem. Lett. 1 (2010). https://doi: 10.1021/jz100889u.

[39] C. R. Luna, V. Verdinelli, E. Germán, H. Seitz, M. A. Volpe, C. Pistonesi, and P. V. Jasen, Hydrogen Adsorption and Associated Electronic and Magnetic Properties of Rh-Decorated (8,0) Carbon Nanotubes Using Density Functional Theory, J. Phys. Chem. C 119, (2015). https://doi: 10.1021/acs.jpcc.5b01407.

[40] J. Maultzsch, H. Telg, S. Reich, and C. Thomsen. Radial breathing mode of single-walled carbon nanotubes. Phys. Rev, B 72 (2005) 205438. https://doi.org/10.1103/PhysRevB.72.205438

[41] J. Touzeau, F. Barbault, F. Maurel, and M. Seydou, Insights on porphyrin-functionalized graphene: theoretical study of substituent and metal-center effects on adsorption, Chem. Phys. Lett., 713 (2018) 172-179. https://doi.org/10.1016/j.cplett.2018.10.046

[42] W. Kim, A. Javey, O. Vermesh, O. Wang, Y. M. Li, H. J. Dai, Hysteresis caused by water molecules in carbon nanotube field-effect transistors, *Nano Lett.* 3 (2003) 193. DOI: 10.1021/nl0259232

[43] S. J. Tans, A. R. M. Verschueren, C. Dekker, Room-temperature transistor based on a single carbon nanotube, Nature 393 (1998) 49-52. https://*doi*.org/10.1038/29954.

[44] F. D'Souza, O. Ito, Photoinduced electron transfer in supramolecular systems of fullerenes functionalized with ligands capable of binding to zinc porphyrins and zinc phthalocyanines, Coord. Chem. Rev., 249 (2005) 1410-1422. https://doi.org/10.1016/j.ccr.2005.01.002

[45] D. M. Guldi, G. N. A. Rahman, J. Ramey, M. Marcaccio, D. Paolucci, F. Paolucci, S. H. Qin, W. T. Ford, D. Balbinot, N. Jux, N. Tagmatarchis, M. Prato, Donor–acceptor nanoensembles of soluble carbon nanotubes, Chem. Commun., (2004) 2034-2035. https://doi.org/10.1039/B406933A